Journal of Physics: Condensed Matter

PAPER

Stability, elastic and electronic properties of a novel BN_2 sheet with extended hexagons with N–N bonds

To cite this article: Kevin Waters and Ravindra Pandey 2018 *J. Phys.: Condens. Matter* **30** 135002

IOP Publishing Journal of Physics: Condensed Matter
J. Phys.: Condens. Matter **30** (2018) 135002 (8pp) https://doi.org/10.1088/1361-648X/aaad96

Stability, elastic and electronic properties of a novel BN_2 sheet with extended hexagons with N–N bonds

Kevin Waters and Ravindra Pandey

Department of Physics, Michigan Technological University, Houghton, MI 49931, United States of America

E-mail: kwaters@mtu.edu and pandey@mtu.edu

Received 6 December 2017, revised 1 February 2018
Accepted for publication 7 February 2018
Published 6 March 2018

Abstract

A new B–N monolayer material (BN_2) consisting of a network of extended hexagons is predicted using density functional theory. The distinguishable nature of this 2D material is found to be the presence of the bonded N atoms (N–N) in the lattice. Analysis of the phonon dispersion curves show this phase of BN_2 to be stable. The calculated elastic properties exhibit anisotropic mechanical properties that surpass graphene in the armchair direction. The BN_2 monolayer is metallic with in-plane p states dominating the Fermi level. Novel applications resulting from a strong anisotropic mechanical strength together with the metallic properties of the BN_2 sheet with the extended hexagons with N–N bonds may enable future innovation at the nanoscale.

Keywords: 2D materials, elastic constants, electronic structure, density functional theory, mechanical properties

(Some figures may appear in colour only in the online journal)

1. Introduction

The 'materials by design' approach using state-of-the-art computational tools has led to new experimental discoveries that have pushed the forefronts of materials science. In recent years, this approach has generated deeper insight into the physics and chemistry of next generation materials with the help of tools and resources which allow for high-throughput calculations with utilities such as genetic and particle-swarm algorithms (Wang *et al* 2012, Ping *et al* 2013). Furthermore, there exists a wealth of knowledge on the structures of known materials which subsequently has led to suggest new combinations of atoms to create new materials that are stable and can then be synthesized.

Theory has anticipated many new materials which were synthesized in scientific laboratories. An example of this is the academic discussion of Dirac cones in monolayer graphite (DiVincenz and Mele 1984). Twenty years later the discovery of what we know now as graphene was announced (Novoselov *et al* 2004). White graphene referred to as a h-BN monolayer, soon followed with theoretical predictions (Wirtz *et al* 2006) and then its synthesis (Jin *et al* 2009, Gorbachev *et al* 2011). More recently this tradition has continued with borophene, first predicted in 2014 by Piazza *et al* (2014) and then synthesized in 2015 by Mannix *et al* (2015). Materials, outside of the B–C–N group, have also been predicted and synthesized, e.g. silicene (Guzmán-Verri and Voon 2007, Fleurence *et al* 2012, Vogt *et al* 2012).

The foundation for the 2D family of the B–C–N materials was set with the discovery of both graphene and the h-BN monolayer. Since then numerous materials in the B–N family have been predicted using first-principles methods based on density functional theory. Some of the carbon-based 2D materials include α graphyne/BNyne (Ozcelik and Ciraci 2013), 6-6-12 graphyne hetero-structures (Malko *et al* 2012), and graphdiyne (Li *et al* 2014). Due to the similar chemistry, between C atoms and B/N atoms, many of the carbon-based materials also have B–N analogues (Li *et al* 2016). Following the prediction of penta-graphene (Zhang *et al* 2015), the stability of BN sheets with similar structures, penta-BN and penta-BN_2, have been reported (Li *et al* 2016). These structures form pentagons with penta-BN having B–N, B–B and N–N bonds with semiconducting properties. On the other

hand, penta-BN_2 shares a similar morphology as penta-BN, but with N–N bonds with metallic properties.

Following the pentagonal and hexagonal structures of B–C–N materials, we now consider a network of extended hexagons with N–N bonds forming a BN_2 monolayer. There is, however, a reduction in symmetry that allows for the anisotropic nature of the material's mechanical properties. Calculations based on density functional theory (DFT) find this BN_2 structure to be stable. Note that these extended hexagons are not regular hexagons typically associated with graphene, and the bonded nitrogen atoms (N–N) modify the hexagon structure of the h-BN monolayer. In the following section, we will briefly describe the computational method and the results are discussed in section 2. A summary of the results is given in section 3.

2. Computational model

Electronic structure calculations were performed using the generalized gradient approximation to DFT. The Perdew–Burke–Ernzerhof (PBE) functional with projector-augmented-wave pseudo-potentials (Blöchl 1994, Kresse 1999) as implemented in the Vienna *Ab initio* Simulation Package (VASP) (Kresse and Hafner 1993, Kresse and Hafner 1994, Kresse 1996, Kresse and Furthmüller 1996) were used. The plane wave cutoff energy was set to 900 eV. The convergence criteria for the energy was set to 10^{-5} eV, while the force was to set to 10^{-4} eV Å^{-1}. The Brillioun zone was sampled with a $(7 \times 21 \times 1)$ Monkhorst–Pack grid (Pack and Monkhorst 1976) for the monolayer and bilayer calculations. For the density of states calculations Gaussian smearing was set to 0.05 eV, and the k-point grids were increased by a factor of four in all directions. Bader's charge analysis was performed using the code and methods given by Henkelman *et al* (2006). Note that the semi-empirical VDW correction terms (D3) (Grimme *et al* 2010) were added for the bilayer BN_2 calculations.

To investigate the stability of the BN_2 monolayer, a larger supercell $(2 \times 2 \times 1)$ was generated for calculations of the force constants, which was then used by the Phonopy software (Togo and Tanaka 2015). The energy convergence criterion in the VASP calculations were increased to 10^{-8} eV to obtain the Hessian matrix for the Phonopy calculations. For structure symmetry identification and high symmetry points, the Bilbao crystallographic server (Aroyo *et al* 2006a, 2006b, Aroyo *et al* 2011, Tasci *et al* 2012, Aroyo *et al* 2014) and utilities within the Pymatgen library (Ping *et al* 2013) were used.

The cohesive energy of a monolayer was calculated using the following formula:

$$E_{\text{cohesive}} = \frac{E_{\text{struc.}} - nE_B - mE_N}{n+m}. \tag{1}$$

The interlayer binding energy for the bilayer was calculated using the following:

$$E_{\text{Binding}} = E_{\text{Bilayer}} - 2E_{\text{Monolayer}}. \tag{2}$$

To calculate the elastic constants the Pymatgen library (Ping *et al* 2013) was utilized to apply the strain to the structures yielding stress–strain data for both the monolayer and bilayer. For the monolayer, the calculation of the in-plane Young's modulus involved steps in which the stresses were multiplied by the cell thickness (c), following the procedures of Wei *et al* (2009) and Peng *et al* (2012). The lattice parameter varied with a strain (ϵ) of -2.0% to 2.0% with a mesh of 0.2% and -1.0% to 1.0% with a mesh of 0.1% for the off-diagonal components. This approach resulted in 20 calculations for each direction of deformation in the lattice. Larger strains were considered, but 2.0% was chosen to limit the stress–strain relationship to a linear regime, as was done in previous studies (Wei and Peng 2014, Mannix *et al* 2015).

To calculate the elastic constants the following formula was used:

$$\boldsymbol{\sigma_{ij}} = \boldsymbol{C_{ijkl}}\boldsymbol{\eta_{kl}} \tag{3}$$

where $\boldsymbol{\sigma_{ij}}$ is the 3x3 stress matrix (Cauchy in this case), $\boldsymbol{C_{ijkl}}$ is the stiffness tensor, and η_{kl} is a 3x3 strain matrix. Using Voigt notation the indices can be reduced to Nye (1985):

$$\boldsymbol{\sigma_I} = \boldsymbol{C_{IJ}}\boldsymbol{\eta_J} \tag{4}$$

where $\boldsymbol{\eta}$ is calculated using the following:

$$\boldsymbol{\eta} = \frac{1}{2}(\boldsymbol{F^T F} - \boldsymbol{I}) \tag{5}$$

where $\boldsymbol{F}$ is the deformation gradient tensor and $\boldsymbol{I}$ is the identity matrix. Solving for the elastic constants $\boldsymbol{C_{IJ}}$ we get:

$$\left[\boldsymbol{\sigma_I}\eta_J^+\right]^T \approx \boldsymbol{C_{IJ}} \tag{6}$$

where $\boldsymbol{\eta_J^+}$ is calculated using the Moore–Penrose pseudo-inverse as implemented in the NumPy library (van der Walt *et al* 2011). Due to the least square fitting, $\approx$ is used to imply that an exact solution is not found.

The deformation gradient tensors for the orthorhombic case are Mouhat and Coudert (2014):

$$\begin{aligned}
\boldsymbol{F_{11}} &= \begin{bmatrix} \lambda_{11} & 0 & 0 \\ 0 & 1 & 0 \\ 0 & 0 & 1 \end{bmatrix} \quad \boldsymbol{F_{22}} = \begin{bmatrix} 1 & 0 & 0 \\ 0 & \lambda_{22} & 0 \\ 0 & 0 & 1 \end{bmatrix} \quad \boldsymbol{F_{33}} = \begin{bmatrix} 1 & 0 & 0 \\ 0 & \lambda_{33} & 0 \\ 0 & 0 & 1 \end{bmatrix} \\
\boldsymbol{F_{44}} &= \begin{bmatrix} 1 & 0 & 0 \\ 0 & \lambda_{44} & 0 \\ 0 & 0 & \lambda_{44} \end{bmatrix} \quad \boldsymbol{F_{55}} = \begin{bmatrix} \lambda_{55} & 0 & 0 \\ 0 & 1 & 0 \\ 0 & 0 & \lambda_{55} \end{bmatrix} \quad \boldsymbol{F_{66}} = \begin{bmatrix} \lambda_{66} & 0 & 0 \\ 0 & \lambda_{66} & 0 \\ 0 & 0 & 1 \end{bmatrix} \\
\boldsymbol{F_{12}} &= \begin{bmatrix} 1 & \epsilon_{12} & 0 \\ 0 & 1 & 0 \\ 0 & 0 & 1 \end{bmatrix} \quad \boldsymbol{F_{13}} = \begin{bmatrix} 1 & 0 & \epsilon_{13} \\ 0 & 1 & 0 \\ 0 & 0 & 1 \end{bmatrix} \quad \boldsymbol{F_{23}} = \begin{bmatrix} 1 & 0 & 0 \\ 0 & 1 & \epsilon_{23} \\ 0 & 0 & 1 \end{bmatrix}
\end{aligned} \tag{7}$$

where $\lambda_{11} = 1 + \epsilon_{11}$, $\lambda_{22} = 1 + \epsilon_{22}$, etc.

Using symmetry the stiffness tensor can be reduced to reflect the unique elements needed to describe an orthorhombic system. The matrix is symmetric across the diagonal and only the unique elements are given in equation (8)

$$C_{IJ} = \begin{bmatrix} C_{11} & C_{12} & C_{13} & 0 & 0 & 0 \\ & C_{22} & C_{23} & 0 & 0 & 0 \\ & & C_{33} & 0 & 0 & 0 \\ & & & C_{44} & 0 & 0 \\ & & & & C_{55} & 0 \\ & & & & & C_{66} \end{bmatrix}. \tag{8}$$

For the monolayer case the matrix in equation (8) is reduced from nine (C_{IJ}) constants to four (C_{IJ}) constants. The deformation gradient tensor $\boldsymbol{F_{11}}$, $\boldsymbol{F_{22}}$, $\boldsymbol{F_{12}}$ and $\boldsymbol{F_{66}}$ are used to apply uniaxial ($\boldsymbol{F_{11}}$,$\boldsymbol{F_{22}}$), shear strain ($\boldsymbol{F_{12}}$) and biaxial ($\boldsymbol{F_{66}}$) strain to the monolayer. With the reduction of elements due to symmetry and dimensionality, the following are the stiffness tensor for the isotropic (left) graphene and h-BN monolayer systems and the anisotropic (right) BN_2 systems (Nye 1985) :

$$C_{\text{iso.}} = \begin{bmatrix} C_{11} & C_{12} & 0 \\ & C_{11} & 0 \\ & & \frac{C_{11}-C_{12}}{2} \end{bmatrix} \quad C_{\text{ani.}} = \begin{bmatrix} C_{11} & C_{12} & 0 \\ & C_{22} & 0 \\ & & C_{66} \end{bmatrix} \tag{9}$$

where the anisotropic in-plane Young's modulus can be calculated using:

$$E_{\text{arm}} = \frac{C_{11}C_{22} - C_{12}C_{12}}{C_{11}}, \quad E_{\text{zig}} = \frac{C_{11}C_{22} - C_{12}C_{12}}{C_{22}}. \tag{10}$$

For the isotropic materials (graphene and h-BN monolayer), where $C_{11} = C_{22}$, the in-plane Young's modulus can be reduced down to the following:

$$E = \frac{C_{11}^2 - C_{12}^2}{C_{11}}. \tag{11}$$

The Poisson ratios are given as:

$$\nu_{xy} = \frac{C_{12}}{C_{22}}, \quad \nu_{yx} = \frac{C_{12}}{C_{11}}. \tag{12}$$

3. Results and discussion

3.1. Monolayer

To establish the reliability and accuracy of the modeling elements, we have first performed calculations on the well-characterized monolayers of graphene and h-BN. The structural, elastic and electronic properties of graphene and h-BN monolayer were well reproduced (table 1) suggesting the reliability of the modeling elements for calculations on BN_2.

Figure 1 displays the equilibrium configuration of the BN_2 monolayer. It consists of a network of hexagons with *Amm*2 (38) symmetry. These hexagons are distinctly different from the regular hexagon shapes associated with the graphene and h-BN monolayers. The unit cell contains two formula units with the lattice parameters of $a = 6.84$ Å and $b = 2.55$ Å. Note that a large value of c (≈19 Å) was used to provide an adequate vacuum distance between the mirror images in the periodic DFT calculations for the BN_2 monolayer. In the equilibrium configuration, the sp^2 bond lengths (R_{B1N2}) are 1.50 Å which is larger than that of a h-BN monolayer (1.45 Å). The bond extending to N_1/N_3 from B_2/B_1 has contracted to a more sp-like character with a distance of 1.34 Å. The shortest bond, 1.29 Å, is between the neighboring nitrogen atoms (N_1/N_2 and N_3/N_4) as shown in figure 1. In the molecular BN_2 with the (B–N–N) configuration, *ab initio* calculations report that the B–N and N–N distances to be 1.51 and 1.15 Å (Martin *et al* 1994). Similarly, the N–N distance is reported to be 1.16, 1.14 and 1.13 Å in AlN_2, GaN_2 and InN_2 molecules (Kandalam *et al* 2000).

Table 1. The calculated lattice parameters of graphene, h-BN, BN_2 and bilayer BN_2. Due to symmetry graphene and h-BN have reduced unique parameters. The atom/bond/angle numbers correspond to figure 1. The interlayer distance for the bilayer is 3.17 Å.

	Graphene	BN	BN_2	BN_2 bilayer
Symmetry (#)	*P*6/*mmm* (191)	*P*$\bar{6}$*m*2 (187)	*Amm*2 (38)	*Amm*2 (38)
Lattice parameters (Å)	$a = 2.47$	$a = 2.51$	$a = 6.84$ $b = 2.55$	$a = 6.84$ $b = 2.55$
Bond length (Å)	C–C	B–N	N_1–N_2 (R_1)	N_1–N_2 (R_1)
	1.42	1.45	1.29	1.29
Bond length (Å)			B_1–N_1 (R_2)	B_1–N_1 (R_2)
			1.50	1.50
Bond length (Å)			B_1–N_2 (R_3)	B_1–N_2 (R_3)
			1.34	1.34
Bond angle (°)	CCC	BNB	$N_2B_1N_2$ (θ_1)	$N_2B_1N_2$ (θ_1)
	120	120	116	116
Bond angle (°)			$N_2B_1N_3$ (θ_2)	$N_2B_1N_3$ (θ_2)
			122	122

To gain a better understanding of the nature of the bonding in this 2D material, calculations of the Bader charges were performed. Figure 1 (right panel) shows a charge of 0.9e (i.e. loss of 2.1e) associated with the B atoms. The N atoms with lower coordination (N_1,N_3) have a charge of 6.0e (i.e. gain of 1.0e), whereas the other nitrogen atoms (N_2,N_4) have a slightly higher charge of 6.1e (i.e. gain of 1.1e). Note that the bonds are more ionic in a h-BN monolayer with the boron and nitrogen having charges of 0.8e (loss of 2.2e) and 7.2e (i.e. gain of 2.2). This bond between N_3 and N_4 atoms will yield the materials high in-plane Young's modulus as shown in the section 3.3.

3.2. Stability

Following equation (1), the calculated cohesive energy (E_{cohesive}) for the BN_2 monolayer is found to be −7.64 eV/unit cell. In comparison, the calculated E_{cohesive} values of graphene and h-BN monolayers are −9.26 and −8.79 eV/unit cell. The BN_2 monolayer with the N–N bond appears to be stable at the PBE-DFT level of theory. Note that *ab initio* calculations suggest the kinetic factors to determine the stability of BN_2 as a molecule with the (B–N–N) configuration (Martin *et al* 1994).

To further establish the stability of the BN_2 monolayer, phonon calculations are performed. The calculated phonon dispersion relationship is shown in figure 2. Accordingly, the BN_2 monolayer is dynamically stable considering that small imaginary frequencies ($\omega < 5$ cm^{-1}) near Γ are likely to be

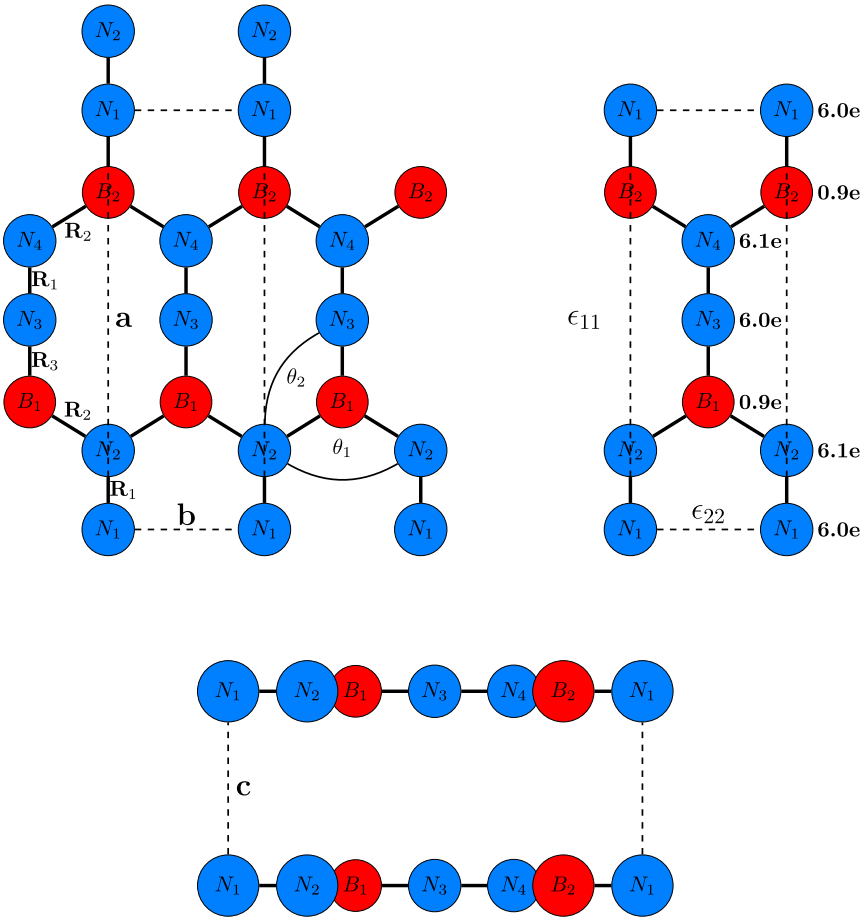

Figure 1. The structure of BN_2 (top left). The unit cell consisting of two B atoms (red) and four N atoms (blue) is outlined with the dashed (–) lines. The lattice parameters, bond lengths and bond angles together with Bader charges on each atom are also listed (table 1). Directions for the applied strain ϵ_{11} and ϵ_{22} are shown. The AA stacked bilayer structure (bottom) is shown with the interlayer distance (c) of 3.17 Å.

due to numerical artifacts that would dissipate if a larger super cell was taken into account or an increase in K-points was considered in calculations. The maximum frequency associated with the optical phonons is about 1700cm^{-1}, which may be associated with the stretching of the N–N bond. The N–N bond stretching mode in AlN_2, GaN_2 and InN_2 molecules is 1887, 2036, and 2094 cm^{-1} (Kandalam *et al* 2000). In contrast, the maximum frequency in the h-BN monolayer is about 1400cm^{-1} associated with the stretching of the B–N bond (Michel and Verberck 2009). For the case of the BN_2 molecule, the highest frequency mode is predicted to be about 1900 cm^{-1} at the *ab initio* level of theory (Martin *et al* 1994). The carbon analogue of the BN_2 monolayer was also investigated, but the presence of large imaginary frequencies ($\omega > 500$ cm^{-1}) suggesting the instability of the carbon analogue.

3.3. Electronic properties

The calculated band structure and density of states find the BN_2 electronic properties to be metallic with the states around the Fermi level are dominated by the in-plane p-orbitals as shown in figure 3. These in-plane orbitals are mainly associated with N_1 and N_3 atoms with smaller contributions from N_2, N_4 and B atoms (figure 1) . Note that the nitrogen atoms (N_1 and N_3) do not show a sp^2 coordination in the lattice. This is in contrast to the case of the h-BN monolayer for which all atoms are all sp^2 coordinated with network of alternating occupied out-of-plane p_z orbitals that do not overlap. In graphene, however, the out-of-plane p_z orbitals give its conducting properties. This can be shown in figure 4 with the electron clouds of graphene and BN_2 being delocalized and h-BN is localized on the nitrogen atom. We find that the metallic properties exhibited by BN_2 can be attributed to the bonded nitrogen atoms (N–N) in the lattice. This metallic behavior is similar to what has been reported for penta-BN_2 (Li *et al* 2016).

3.4. Elastic properties

Table 2 lists the calculated values of the elastic constants and Poisson's ratios for BN_2, together with those of graphene and the h-BN monolayer. First, we find a noticeable feature associated with BN_2 which shows the anisotropic behavior with the elastic constants being $C_{11} = 368.8$ N m^{-1}, $C_{12} = 47.2$ N m^{-1}, and $C_{22} = 153.3$ N m^{-1}. In the armchair direction, a Young's modulus of 354.3 N m^{-1} is predicted suggesting BN_2 to be stiffer than graphene (343 N m^{-1}) and the h-BN monolayer (276.2 N m^{-1}). In the zig-zag direction, a smaller modules of 147.3 N m^{-1} is predicted. The same trend is exhibited for the Poisson's ratio in

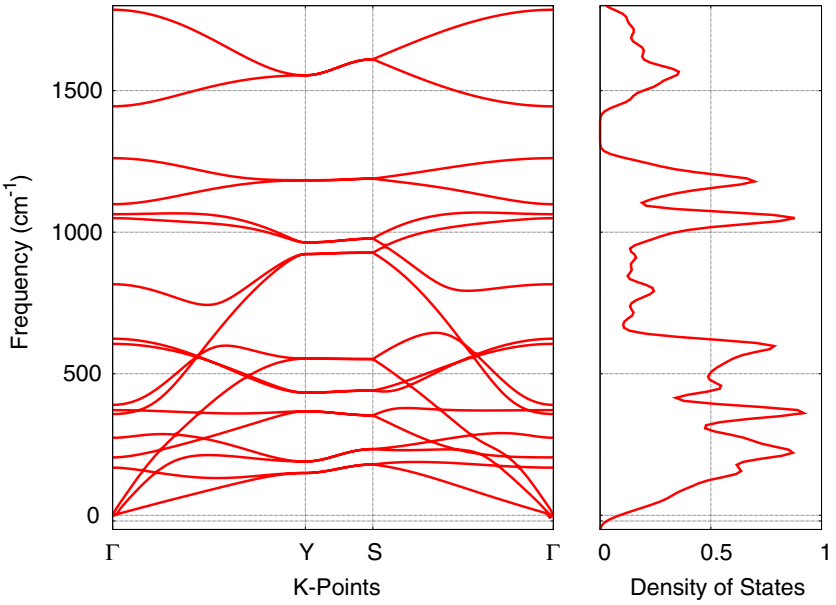

Figure 2. Calculated phonon dispersion (left) and the associated phonon density of states (right) of BN_2.

the zigzag and armchair directions of the BN_2 monolayer. The calculated elastic constants for graphene and the h-BN monolayer are in agreement with the previously reported theoretical results as show in table 2 (Wei *et al* 2009, Peng *et al* 2012). For graphene, our calculated values of the elastic constants agree when compared to experimental work of graphene on metal substrates (Politano and Chiarello 2015). For example, the in-plane Young's modulus of graphene on Pt(1 1 1 1). Ru(0 0 0 1), Ir(1 1 1), BC_3/NbB_2(0 0 0 1) substrates is 342 N m^{-1}.

When compared to other similar 2D materials such as penta-graphene (Zhang *et al* 2015), penta-BN (Li *et al* 2016) and penta-BN_2 (Li *et al* 2016), the BN_2 monolayer appears to be stiffer with a larger Poisson's ratio. The Young's modulus for penta-graphene (Zhang *et al* 2015), penta-BN (Li *et al* 2016), and penta-BN_2 (Li *et al* 2016) are reported to be 263.8, 133, and 224 N m^{-1}.

All previously reported structures are isotropic which leads to $C_{11} = C_{22}$, the directions then have identical Young's moduli and Poisson ratios for the 11 and 22 directions. For the symmetric values, e.g. $C_{11} = C_{22}$, the values are identical, but due to numerical procedures there are slight variations. To address this discrepancy the average of each of these values are presented in table 2. A similar procedure was done for the off-diagonal terms, due to the mirrored terms in the $\boldsymbol{C_{IJ}}$ tensor.

3.5. Bilayer

Next, we considered the case of the bilayer BN_2 stacked in either AA or AB configuration. The AB stacked bilayer configuration was generated by rotating the second layer by 180° with respect to the first layer. The AA stacked bilayer configuration consists of atoms of the first layer are on top of the atoms of the second layer (figure 1). In the equilibrium configuration obtained at the PBE + D3-DFT level of theory, the interlayer distance is calculated to be 3.17 Å for both stacking configurations. The calculated binding energy (equation (2)) of the AA and AB- stacked configuration is found to be −0.28 eV and −0.22 eV suggesting the AA-stacked bilayer to be energetically preferred. The calculated band structure and density of states predict the bilayer to be metallic displaying features similar to those obtained for the monolayer (figure 5).

Table 2. Calculated elastic constants (C_{xx}), in-plane Young's modulus defined in equation (10) ($E_{arm/zig}$), and Poisson's ratio (ν) defined in equation (12) for graphene and monolayers of h-BN and BN_2. C_{66} is computed using strain and stress data. Units are in N m^{-1}, except for ν which is unitless.

	Graphene[a]	This work	BN[b]	This work	BN_2	Bilayer
C_{11}	358.1	353.7	293.2	290.5	368.8	357.7
C_{12}	60.4	61.7	66.1	64.4	47.2	45.5
C_{13}						−5.2
C_{22}					153.3	107.3
C_{23}						−22.7
C_{33}						5.0
C_{44}						0.4
C_{55}						0.4
C_{66}		144.9		113.1	58.7	50.2
E_{Arm}	348	343.0	278.3	276.2	354.3	
E_{Zig}					147.3	
ν_{xy}	0.169	0.17	0.2176	0.22	0.31	0.42
ν_{yx}					0.13	0.13

[a] Wei *et al* (2009)
[b] Peng *et al* (2012).

The bilayer mechanical properties has similar in-plane properties when compared to the monolayer. C_{11} has a difference of about 10 N m^{-1}, C_{12} by about 2 N m^{-1}, C_{66} by about 9 N m^{-1}. The largest difference is in the C_{22} term with a difference of about 45 N m^{-1}. The extra dimension added by the layer requires more elastic constants, which are expected to be small due to the long-ranged interactions (C_{x3}, C_{44}, C_{55}). C_{13} has a value of −5.2 N m^{-1}, C_{23} −22.7 N m^{-1}, C_{33} 5.0 N m^{-1}, C_{44} and C_{55} 0.4 N m^{-1}. The change in C_{22} resulted in a greater value of ν_{xy}, 0.42.

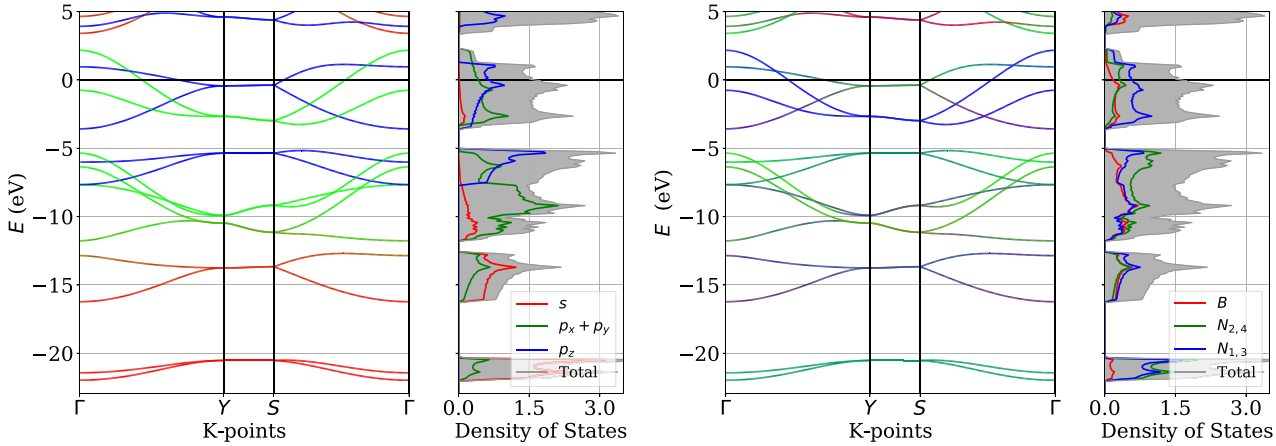

Figure 3. Calculated band structure and density of states of the BN_2 monolayer. (Left) orbital projected color code: blue—s states, green—in-plane p_x and p_y states, blue—out-of-plane p_z states, grey—total density of states. (Right) atomic projected color code: blue—$N_{1,3}$ states, green—$N_{2,4}$ states, red—B states, and grey—total density of states.

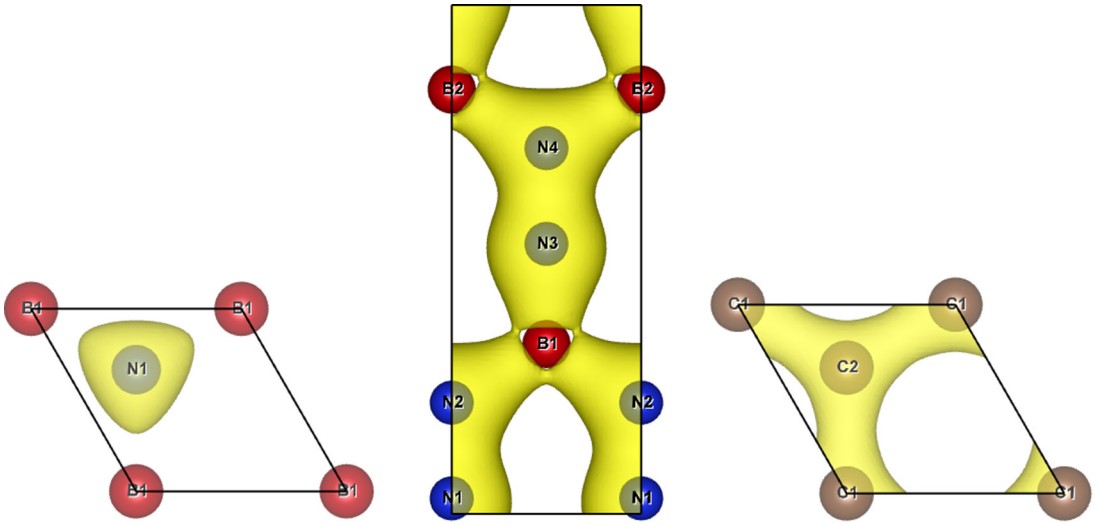

Figure 4. Charge density of BN (left), BN_2 (middle), graphene (right) with an isovalue = 0.2e. The metallic, graphene and BN_2 structures show a delocalized electronic cloud as opposed the localized electronic cloud of the semiconducting h-BN.

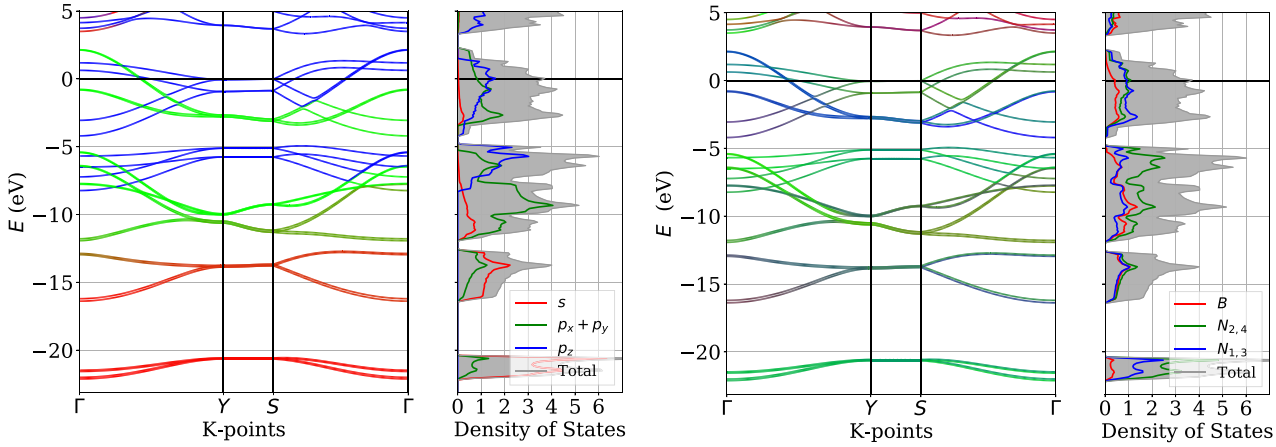

Figure 5. Calculated band structures and density of states of the AA BN_2 bilayer. (Left) orbital projected color code: blue—s states, green—in-plane p_x and p_y states, blue—out-of-plane p_z states, grey—total density of states. (Right) atomic projected color code: blue—$N_{1,3}$ states, green—$N_{2,4}$ states, red—B states, grey—total density of states.

4. Summary

A new B–N monolayer material (BN_2) consisting of a network of extended hexagons was predicted to be stable with a comparable value of the cohesive energy relative to that of the h-BN monolayer. The distinguishable nature of this 2D material was found to be the presence of the bonded N atoms (N–N) in the lattice. The highest phonon frequency carries the signature of the N–N bond in the 2D lattice. The monolayer is predicted to be metallic with in-plane p states dominating the Fermi level. We find that the monolayer exhibits anisotropic mechanical properties that surpass graphene in the armchair direction. This anisotropy may lead to novel applications in the future if some challenges are overcome in the synthesis this material.

Acknowledgments

KW would like to acknowledge Germain Salvato–Vallverdu for the availability of their source codes which was posted on github. The Pymatgen scripts framework provided were utilized and built off of for some of the figures presented in the manuscript. Superior, a high performance computing cluster at Michigan Technological University, was used in obtaining the results presented in this publication.

ORCID iDs

Kevin Waters https://orcid.org/0000-0003-3828-8647
Ravindra Pandey https://orcid.org/0000-0002-2126-1985

References

Aroyo M I, Kirov A, Capillas C, Perez-Matoa J M and Wondratschekc H 2006a Bilbao crystallographic server. II. Representations of crystallographic point groups and space groups *Acta Crystallogr. Sect.* A **62** 115
Aroyo M I, Perez-Mato J M, Orobengoa D, Tasci E, de la Flor G and Kirov A 2011 Crystallography online: Bilbao crystallographic server *Bulg. Chem. Commun.* **43** 183
Aroyo M I, Perez-Matoa J M, Capillas C, Kroumova E, Ivantchev S, Madariaga G, Kirov A and Wondratschekc H 2006b Bilbao crystallographic server: I. Databases and crystallographic computing programs *Z. Kristallogr.* **221** 15
Aroyo M, Orobengoa D, de la Flor G, Tasci E S, Perez-Matoa J M and Wondratschekc H 2014 Brillouin-zone database on the Bilbao crystallographic server *Acta Crystallogr. Sect.* A **70** 126
Blöchl P E 1994 Projector augmented-wave method *Phys. Rev.* B **50** 17953–79
DiVincenz D P and Mele E J 1984 Self-consistent effective-mass theory *Phys. Rev.* B **29** 1685
Fleurence A, Friedlein R, Ozaki T, Kawai H, Wang Y and Yamada-Takamura Y 2012 Experimental evidence for epitaxial silicene on diboride thin films *Phys. Rev. Lett.* **108** 245501
Gorbachev R V *et al* 2011 Hunting for monolayer boron nitride: optical and Raman signatures *Small* **7** 465
Grimme S, Antony J, Ehrlich S, Krieg H, Grimme S, Antony J, Ehrlich S and Krieg H 2010 A consistent and accurate *ab initio* parametrization of density functional dispersion correction (DFT-D) for the 94 elements H-Pu *J. Chem. Phys.* **132** 154104
Guzmán-Verri G G and Voon L C L Y 2007 Electronic structure of silicon-based nanostructures *Phys. Rev.* B **76** 075113
Henkelman G, Arnaldsson A and Jonsson H 2006 A fast and robust algorithm for Bader decomposition of charge density *Comput. Mater. Sci.* **36** 354
Jin C, Lin F, Suenaga K and Iijima S 2009 Fabrication of a freestanding boron nitride single layer and its defect assignments *Phys. Rev. Lett.* **102** 195505
Kandalam A, Pandey R, Blanco M A, Costales A, Recio M and Newsam J N 2000 First principles study of polyatomic clusters of AlN, GaN, and InN. 1. Structure, stability, vibrations, and ionization *J. Phys. Chem.* B **104** 4361
Kresse G 1996 Efficient iterative schemes for *ab initio* total-energy calculations using a plane-wave basis set *Phys. Rev.* B **54** 11169
Kresse G 1999 From ultrasoft pseudopotentials to the projector augmented-wave method *Phys. Rev.* B **59** 1758
Kresse G and Furthmüller J 1996 Efficiency of *ab initio* total energy calculations for metals and semiconductors using a plane-wave basis set *Comput. Mater. Sci.* **6** 15
Kresse G and Hafner J 1994 *Ab initio* molecular-dynamics simulation of the liquid-metalamorphous-semiconductor transition in germanium *Phys. Rev.* B **49** 14251–69
Kresse G and Hafner J 1993 *Ab initio* molecular dynamics for liquid metals *Phys. Rev.* B **47** 558
Li J, Fan X, Wei Y and Chen G 2016 Penta-B_xN_y sheet: a density functional theory study of two-dimensional material *Sci. Rep.* **6** 31840
Li Y, Xu L and Li Y 2014 Graphdiyne and graphyne: from theoretical predictions to practical construction *Chem. Soc. Rev.* **43** 2572
Malko D, Neiss C and Andreas G 2012 Two-dimensional materials with Dirac cones: graphynes containing heteroatoms *Phys. Rev.* B **86** 045443
Mannix A J *et al* 2015 Synthesis of borophenes: anisotropic, two-dimensional boron polymorphs *Science* **350** 1513
Martin J M L, Taylor P R, Francois J P and Gijbels R 1994 *Ab initio* study of the spectroscopy, kinteics, and thermochemistry of the BN_2 molecule *Chem. Phys. Lett.* **222** 517
Michel K H and Verberck B 2009 Theory of elastic and piezoelectric effects in two-dimensional hexagonal boron nitride *Phys. Rev.* B **80** 224301
Mouhat F and Coudert F X 2014 Necessary and sufficient elastic stability conditions in various crystal systems *Phys. Rev.* B **90** 224104
Novoselov K S, Geim A K, Morozov S V, Jiang D, Zhang Y, Dubonos S V, Grigorieva I V and Firsov A A 2004 Electric field effect in atomically thin carbon films *Science* **306** 666
Nye J F 1985 *Physical Properties of Crystals* (Oxford: Oxford University Press)
Ozcelik V O and Ciraci S 2013 Size dependence in the stabilities and electronic properties of α graphyne and its boron nitride analogue *J. Phys. Chem.* C **117** 2175
Pack J D and Monkhorst H J 1976 Special points for Brillouin-zone integrations *Phys. Rev.* B **16** 1748–9
Peng Q, Ji W and De S 2012 Mechanical properties of the hexagonal boron nitride monolayer: *ab initio* study *Comput. Mater. Sci.* **56** 11
Piazza Z A, Hu H S, Li W L, Zhao Y F, Li J and Wang L S 2014 Planar hexagonal B36 as a potential basis for extended single-atom layer boron sheets *Nat. Commun.* **5** 1
Ping S, Davidson W, Jain A, Hautier G, Kocher M, Cholia S, Gunter D, Chevrier V L, Persson K A and Ceder G 2013 Python materials genomics (pymatgen): a robust, open-source python library for materials analysis *Comput. Mater. Sci.* **68** 314
Politano A and Chiarello G 2015 Probing the Young's modulus and Poisson's ratio in graphene / metal interfaces and graphite: a comparative *Nano Res.* **8** 1847

Tasci E, de la Flor G, Orobengoa D, Capillas C, Perez-Mato J and Aroyo M 2012 An introduction to the tools hosted in the Bilbao crystallographic server *EPJ Web Conf.* **22** 00009

Togo A and Tanaka I 2015 First principles phonon calculations in materials science *Scr. Mater.* **108** 1

van der Walt S, Colbert S C and Varoquaux G 2011 The NumPy array: a structure for efficient numerical computation *Comput. Sci. Eng.* **13** 22

Vogt P, Padova P D, Quaresima C, Avila J, Frantzeskakis E, Lay G L, Asensio M C and Resta A 2012 Silicene: compelling experimental evidence for graphene-like two-dimensional silicon *Phys. Rev. Lett.* **108** 155501

Wang Y, Lv J, Zhu L and Ma Y 2012 CALYPSO: a method for crystal structure prediction *Comput. Phys. Commun.* **183** 2063

Wei Q and Peng X 2014 Superior mechanical flexibility of phosphorene and few-layer black phosphorus *Appl. Phys. Lett.* **104** 251915

Wei X, Fragneaud B, Marianetti C A and Kysar J W 2009 Nonlinear elastic behavior of graphene: *ab initio* calculations to continuum description *Phys. Rev.* B **80** 205407

Wirtz L, Marini A and Rubio A 2006 Excitons in boron nitride nanotubes: dimensionality effects *Phys. Rev. Lett.* **96** 126104

Zhang S, Zhou J, Wang Q, Chen X, Kawazoe Y and Jena P 2015 Penta-graphene: a new carbon allotrope *Proc. Natl Acad. Sci. USA* **112** 2372